

1 **Bacteria boost mammalian host NAD metabolism by engaging the deamidated biosynthesis**  
2 **pathway**

3

4 Short title: Bacteria-host crosstalk in NAD metabolism

5

6 One sentence summary: bacteria boost host NAD metabolism and confer host with resistance to  
7 NAMPT inhibitors

8

9 Igor Shats<sup>1,\*</sup>, Juan Liu<sup>2</sup>, Jason G. Williams<sup>3</sup>, Leesa J. Deterding<sup>3</sup>, Chaemin Lim<sup>4</sup>, Ethan Lee<sup>1</sup>,  
10 Wei Fan<sup>1</sup>, Marina Sokolsky<sup>4</sup>, Alexander V. Kabanov<sup>4</sup>, Jason W. Locasale<sup>2</sup> and Xiaoling Li<sup>1,\*</sup>

11

12 <sup>1</sup>Signal Transduction Laboratory and <sup>3</sup>Mass Spectrometry Research and Support Group,  
13 Epigenetics and Stem Cell Biology Laboratory

14 National Institute of Environmental Health Sciences, Research Triangle Park, NC 27709, USA.

15 <sup>2</sup>Department of Pharmacology and Cancer Biology, Duke University School of Medicine,  
16 Durham, NC 27710, USA.

17 <sup>4</sup>Center for Nanotechnology in Drug Delivery, University of North Carolina, Chapel Hill, NC  
18 27514, USA.

19

20

21

22

23 \* Corresponding authors: [igor.shats@nih.gov](mailto:igor.shats@nih.gov) (I.S.), [lix3@niehs.nih.gov](mailto:lix3@niehs.nih.gov) (X.L.)

24 **Abstract**

25 Nicotinamide adenine dinucleotide (NAD), a cofactor for hundreds of metabolic reactions in all  
26 cell types, plays an essential role in diverse cellular processes including metabolism, DNA  
27 repair, and aging <sup>1</sup>. NAD metabolism is critical to maintain cellular homeostasis in response to  
28 the environment, and disruption of this homeostasis is associated with decreased cellular NAD  
29 levels in aging <sup>2</sup>. Conversely, elevated NAD synthesis is required to sustain the increased  
30 metabolic rate of cancer cells <sup>3,4</sup>. Consequently, therapeutic strategies aimed to both upregulate  
31 NAD (i.e. NAD-boosting nutraceuticals) or downregulate NAD (inhibitors of key NAD synthesis  
32 enzymes) are being actively investigated <sup>5-10</sup>. However, how this essential metabolic pathway is  
33 impacted by the environment remains unclear. Here, we report an unexpected trans-kingdom  
34 cooperation between bacteria and mammalian cells wherein bacteria contribute to host NAD  
35 biosynthesis. Bacteria confer cancer cells with the resistance to inhibitors of NAMPT, the rate  
36 limiting enzyme in the main vertebrate NAD salvage pathway. Mechanistically, a microbial  
37 nicotinamidase (PncA) that converts nicotinamide to nicotinic acid, a key precursor in the  
38 alternative deamidated NAD salvage pathway, is necessary and sufficient for this protective  
39 effect. This bacteria-enabled resistance mechanism that allows the mammalian host to bypass  
40 the drug-induced metabolic block represents a novel paradigm in drug resistance. This host-  
41 microbe metabolic interaction also enables bacteria to dramatically enhance the NAD-boosting  
42 efficiency of nicotinamide supplementation *in vitro* and *in vivo*, demonstrating a crucial role of  
43 microbes, gut microbiota in particular, in organismal NAD metabolism.

44

45

46

47  
48 NAD is an essential cofactor in hundreds of redox reactions. It is also consumed by DNA  
49 repair enzymes (i.e. PARPs, poly(adenosine diphosphate– ribose) polymerases) and by protein  
50 deacylases (e.g. sirtuins) to regulate many fundamental cellular processes, including energy  
51 metabolism, genome stability, and circadian rhythms <sup>1</sup>. Mammalian cells are capable of  
52 synthesizing NAD from the amino acid tryptophan (*de novo* pathway) or from nicotinic acid  
53 (NA, Preiss-Halder deamidated salvage pathway). However, the main cellular source of NAD is  
54 its salvage from nicotinamide (NAM, amidated salvage pathway), where nicotinamide  
55 phosphoribosyl transferase (NAMPT) is the rate limiting enzyme <sup>11</sup> (Fig. 1A).

56 Cellular NAD homeostasis buffers the constant perturbations from the environment that  
57 affect NAD levels. Whereas various cell-autonomous regulatory mechanisms have been  
58 described, the impact of microorganisms on mammalian NAD homeostasis remains largely  
59 unknown. We now report a mechanism by which mammalian host NAD metabolism is  
60 maintained through a host-microbe metabolic interaction that we discovered serendipitously.

61 We conducted a chemical screen to identify pharmacologic compounds that induce cell  
62 death through E2F1, a transcription factor the level of which plays a crucial role in determining  
63 cell fate <sup>12</sup>. As shown in Fig. 1B, in a screen of 2300 bioactive compounds, the top hits that killed  
64 wild-type (WT) cells more efficiently than E2F1 knockout (KO) H1299 lung cancer cells were  
65 two NAMPT inhibitors, STF31 and STF118804. E2F1 KO cells were also protected from  
66 toxicity induced by proteasome inhibitors, MLN-2238 and its pro-drug MLN-9708, but were  
67 more sensitive to fludarabine and fludarabine phosphate (Fig. 1B and Table S1). Subsequently,  
68 we found that E2F1 KO cells, but not the WT cells, were contaminated with *Mycoplasma*  
69 *hyorhina*, and the differential responses of WT and E2F1 KO cells to all top hits from our screen

70 were due to mycoplasma contamination rather than E2F1 deficiency (Fig. 1C and Fig. S1).  
71 Particularly, in mycoplasma-free CRC119 colon cancer cells, mycoplasma-containing  
72 supernatant from an infected culture was sufficient to completely prevent toxicity induced by the  
73 two NAMPT inhibitors, STF118804 and STF31, and by the proteasome inhibitor MLN-2238  
74 (Fig. 1C). Mycoplasma also dramatically sensitized the CRC119 cells to fludarabine (Fig. 1C),  
75 likely due to the ability of mycoplasma-encoded purine nucleoside phosphorylases to convert  
76 fludarabine (a pro-drug) to a highly toxic purine base<sup>13</sup>. Chronic infection with *M. hyorhinitis*  
77 purchased from ATCC also protected CRC119 cells from STF118804-induced cell death (Fig.  
78 S2) and conferred resistance to three different NAMPT inhibitors (NAMPTi) in two additional  
79 cell lines (Fig. S3). Conversely, treatment with structurally diverse antibiotics that eliminate *M.*  
80 *hyorhinitis* completely reversed this resistance (Fig. 1D), further confirming that mycoplasma  
81 protects host mammalian cells from NAMPTi-induced cell death. Consistent with these  
82 observations in cultured cells, *M. hyorhinitis*-infected HCT116 xenograft tumors but not the  
83 uninfected tumors were protected against STF118804-induced repression of proliferation genes,  
84 such as Cyclin A2 (CCNA2) and E2F1 (Fig. S4A). Our drug screen was highly specific and  
85 revealed very few strong hits with NAMPT inhibitors being the top hits. This strongly suggested  
86 that NAD metabolism is the main cellular pathway affected by mycoplasma infection.

87 Mycoplasma are common cell culture contaminants and a clinically important component  
88 of the human commensal and pathogenic microbiome in various tissues<sup>14-16</sup>. Mycoplasma  
89 presence has also been reported in various cancer types, however, its functional importance  
90 remains unclear<sup>17</sup>. Given the central role of NAD in normal and tumor energy metabolism, the  
91 fact that NAMPTi were the top hits in our drug screen, and the importance of this drug class as  
92 novel antineoplastic agents, we next sought to elucidate the mechanism underlying mycoplasma-

93 mediated protection from NAMPTi-induced toxicity. We assessed the effects of STF118804  
94 treatment over time and found that mycoplasma attenuated NAD depletion and completely  
95 restored ATP levels (Fig. 1E). Bioenergetic profiling demonstrated that this mycoplasma-  
96 provided protective effect was accompanied by a rescue of cellular glycolysis and oxygen  
97 consumption in STF118804-treated cells (Fig. 1F), suggesting that mycoplasma restore the  
98 cellular NAD pool and oxidative phosphorylation. In particular, mycoplasma rescued the  
99 STF1188804-induced reduction of NAD in isolated mitochondria (Fig. 1G) and rescued  
100 STF118804-induced loss of mitochondrial membrane potential (Fig. 1H). Therefore,  
101 mycoplasma infection prevents NAMPTi-induced energy depletion and subsequent cell death by  
102 partially rescuing cellular NAD levels. We showed that similar mechanisms are utilized *in vivo*,  
103 as NAD depletion in HCT116 xenograft tumors following STF118804 treatment was  
104 significantly attenuated in mycoplasma-infected tumors (Fig. S4B).

105 To further uncover the molecular basis of this mycoplasma-provided protective effect on  
106 cellular NAD metabolism, we performed metabolomic analyses of uninfected or *M. hyorhinitis*-  
107 infected CRC119 cells treated with STF118804 or DMSO vehicle control. Principal component  
108 analysis (PCA) revealed that STF118804 induced dramatic metabolic alterations in clean human  
109 cells but mycoplasma infection prevented these global changes (Fig. S5A). Remarkably, the top  
110 metabolites differentially induced by mycoplasma in cells were two key intermediate metabolites  
111 in the Preiss-Handler deamidated NAD biosynthesis pathway, nicotinic acid riboside (NAR) and  
112 nicotinic acid adenine dinucleotide (NAAD) (Fig. 2A and 2B). Furthermore, culture medium  
113 from mycoplasma-infected cells contained more than 5-fold higher levels of NA and more than  
114 8-fold higher levels of NAR compared to medium from uninfected clean cells (Fig. 2B and S5B),  
115 supporting the notion that the increased intracellular levels of NAR and NAAD originated from

116 the increased extracellular NA or NAR. Notably, intracellular STF118804 levels were not  
117 affected by mycoplasma (Fig. S5C), indicating that mycoplasma neither degrade STF118804,  
118 unlike the reported mechanism of direct drug degradation by bacteria in the case of gemcitabine  
119 <sup>18</sup>, nor inhibit the cellular uptake of this compound.

120 Further analyses unveiled that the mycoplasma-induced increase in the Preiss-Handler  
121 deamidated NAD biosynthesis pathway was associated with significant rescue of cellular NAD  
122 levels after STF118804 treatment (Fig. 2B and 2C). In particular, STF118804 treatment resulted  
123 in a 99.6% drop of cellular NAD levels in clean cells within 24 hours, compared with an 88%  
124 drop in mycoplasma-infected cells (Fig. 2C, NAD). We hypothesized that this mycoplasma-  
125 mediated partial rescue of cellular levels of NAD (from 0.4% to 12%) is sufficient to sustain the  
126 cellular energy metabolism upon treatment with NAMPTi. Consistent with this notion, pathway  
127 analysis of differential metabolites in mycoplasma-infected vs. clean STF118804-treated cells  
128 identified the TCA cycle as the most significant metabolic pathway rescued by mycoplasma (Fig.  
129 S5D). In addition, STF118804 treatment resulted in a complete block of glycolysis at the NAD-  
130 dependent GAPDH step in uninfected cells (Fig. 2D, left). Importantly, the STF118804-induced  
131 block of glycolysis was rescued and the changes in the TCA cycle were attenuated in  
132 mycoplasma-infected cells (Fig. 2D, right). Taken together, our results indicate that mycoplasma  
133 primarily affect NAD-mediated energy metabolism in host cells.

134 The amidated (via NAM) and deamidated (via NA) salvage pathways of NAD  
135 biosynthesis are isolated in vertebrate cells due to lack of a nicotinamidase activity that converts  
136 NAM to NA (Fig. 1A). In contrast, multiple bacteria species encode nicotinamidases <sup>19</sup>. Given  
137 the dramatic upregulation of the deamidated NAD precursors (NA and NAR) in mycoplasma-  
138 infected medium and cells (Fig. S5B and 2B), we hypothesized that protection from NAMPTi by

139 mycoplasma (and possibly other bacteria) may be mediated by bacterial nicotinamidase PncA,  
140 which can bypass the NAMPT block by diverting NAM to the deamidated route of NAD  
141 biosynthesis. In support of this hypothesis, we found that *E. coli*, like mycoplasma, protected  
142 CRC119 cells from toxicity of two different NAMPT inhibitors, STF118804 and FK866 (Fig.  
143 3A). This protection was also accompanied by partial rescue of STF118804-induced NAD  
144 depletion in both the cytosol and mitochondria (Fig. S6A) and restoration of both glycolysis and  
145 oxidative phosphorylation (Fig. S6B). Importantly, deletion of the *E. coli pncA* gene completely  
146 abolished this rescue effect (Fig. 3B). Rescue of viability of NAMPTi-treated cells could also be  
147 achieved by addition of conditioned medium (CM) from WT *E. coli* incubated with NAM but  
148 not by CM from WT *E. coli* incubated without NAM (Fig. 3C). We detected robust conversion  
149 of NAM to NA by *E. coli* in the medium by LC-MS (Fig. S7). Direct supplementation of NA, the  
150 product of the PncA enzyme, into culture medium also rescued clean cells from STF118804  
151 toxicity (Fig. 3D). Furthermore, overexpression of *E. coli* PncA in CRC119 cells was sufficient  
152 to completely rescue them from STF118804-induced death (Fig. S6C and 3E). In contrast,  
153 blocking the deamidated NAD biosynthesis by a NAPRT inhibitor, 2-hydroxynicotinic acid  
154 (HNA), abolished the protection from NAMPTi mediated by both *E. coli* and *M. hyorhinis* (Fig.  
155 3F).

156 Finally, supplementation of bacteria-containing culture medium with isotopically labeled  
157 NAM resulted in a robust incorporation of the label into intracellular NA, NAR, NAAD and  
158 NAD even when NAMPT was inhibited by STF118804 (Fig. 4A and S6D), demonstrating that  
159 *E. coli* and *M. hyorhinis* are capable of converting NAM to NA and promoting the deamidated  
160 route of NAD biosynthesis in host cells. In line with this *in vitro* observation, isotopically labeled  
161 NAM was rapidly converted to NA and NAAD in the colons when gavaged into microbiota-

162 proficient regular mice (Fig. 4B and 4C, Reg NAM), but this conversion was severely blunted in  
163 antibiotic-treated microbiota-depleted mice (Fig. 4C, Abx NAM, Fig. 4D, and Fig. S8).  
164 Moreover, in agreement with the previous studies <sup>6</sup>, NAM supplementation led to more than  
165 100-fold increase in the liver NAAD and a 2.5-fold increase in liver NAD in conventional mice.  
166 However, this accumulation of NAAD was abolished and NAD boost was severely attenuated in  
167 the livers of antibiotic-treated mice (Figs. 4C and 4D). These results suggest a model in which  
168 gut bacteria deamidate dietary NAM to NA, which is then converted to NAAD in gut cells.  
169 NAAD is further transported to the liver, where it significantly contributes to hepatic NAD  
170 biosynthesis (Fig. 4D).

171 Collectively, our results demonstrate that bacteria enhance host mammalian cell NAD  
172 metabolism by engaging the deamidated route of NAD biosynthesis *in vitro* and *in vivo*, and that  
173 this metabolic crosstalk is one of the major interactions between host cells and bacteria. Given  
174 the recently reported presence of intratumor bacteria, including mycoplasma, in multiple tumor  
175 types <sup>14,18</sup>, bacteria-mediated resistance described here may have contributed to the failure of  
176 NAMPT inhibitors in cancer clinical trials. This finding suggests co-treatment of NAMPT  
177 inhibitors with antibiotics as a potential novel therapeutic strategy. Our finding further suggests  
178 that development of specific PncA inhibitors for concomitant use with NAMPT inhibitors may  
179 provide an even more specific approach to avoid complete microbiome depletion and other  
180 undesired side effects of antibiotics. Finally, as commonly used NAD-increasing nutraceuticals  
181 nicotinamide mononucleotide and nicotinamide riboside are quickly degraded to nicotinamide  
182 after administration <sup>20</sup>, bacteria-mediated dramatic facilitation of the NAD-boosting activity of  
183 NAM supplementation (Fig. 4) demonstrates a crucial role for microbes, particularly gut  
184 microbiota, in mediating the efficiency of NAD-increasing nutraceuticals.





186 **References**

187

- 188 1. Cantó, C., Menzies, K. J. & Auwerx, J. NAD<sup>+</sup> Metabolism and the Control of Energy  
189 Homeostasis: A Balancing Act between Mitochondria and the Nucleus. *Cell Metab.* **22**,  
190 31–53 (2015).
- 191 2. Imai, S. & Guarente, L. NAD<sup>+</sup> and sirtuins in aging and disease. *Trends Cell Biol.* **24**,  
192 464–471 (2014).
- 193 3. Roulston, A. & Shore, G. C. New strategies to maximize therapeutic opportunities for  
194 NAMPT inhibitors in oncology. *Mol. Cell. Oncol.* **3**, e1052180 (2016).
- 195 4. Hong, S. M. *et al.* Increased NAD(H) pool promotes colon cancer progression by  
196 suppressing ROS level. *Cancer Sci.* (2018). doi:10.1111/cas.13886
- 197 5. Martens, C. R. *et al.* Chronic nicotinamide riboside supplementation is well-tolerated and  
198 elevates NAD<sup>+</sup> in healthy middle-aged and older adults. *Nat. Commun.* **9**, 1286 (2018).
- 199 6. Trammell, S. A. J. *et al.* Nicotinamide riboside is uniquely and orally bioavailable in mice  
200 and humans. *Nat. Commun.* **7**, (2016).
- 201 7. Uddin, G. M., Youngson, N. A., Doyle, B. M., Sinclair, D. A. & Morris, M. J.  
202 Nicotinamide mononucleotide (NMN) supplementation ameliorates the impact of  
203 maternal obesity in mice: comparison with exercise. doi:10.1038/s41598-017-14866-z
- 204 8. Yoshino, J., Baur, J. A. & Imai, S.-I. NAD<sup>+</sup> Intermediates: The Biology and Therapeutic  
205 Potential of NMN and NR. *Cell Metab.* **0**, (2017).
- 206 9. Das, A. *et al.* Impairment of an Endothelial NAD<sup>+</sup>-H<sub>2</sub>S Signaling Network Is a  
207 Reversible Cause of Vascular Aging. *Cell* **173**, 74–89.e20 (2018).
- 208 10. Chen, H., Wang, S., Zhang, H., Nice, E. C. & Huang, C. Nicotinamide

- 209 phosphoribosyltransferase (Nampt) in carcinogenesis: new clinical opportunities. *Expert*  
210 *Rev. Anticancer Ther.* **16**, 827–838 (2016).
- 211 11. Belenky, P., Bogan, K. L. & Brenner, C. NAD<sup>+</sup> metabolism in health and disease. *Trends*  
212 *Biochem. Sci.* **32**, 12–19 (2007).
- 213 12. Shats, I. *et al.* Expression level is a key determinant of E2F1-mediated cell fate. *Cell*  
214 *Death Differ.* **24**, 626–637 (2017).
- 215 13. Vande Voorde, J., Vervaeke, P., Liekens, S. & Balzarini, J. Mycoplasma hyorhinitis-  
216 encoded cytidine deaminase efficiently inactivates cytosine-based anticancer drugs. *FEBS*  
217 *Open Bio* **5**, 634–9 (2015).
- 218 14. Barykova, Y. A. *et al.* Association of Mycoplasma hominis infection with prostate cancer.  
219 *Oncotarget* **2**, 289–297 (2011).
- 220 15. Duan, H. *et al.* Mycoplasma hyorhinitis infection promotes NF- $\kappa$ B-dependent migration of  
221 gastric cancer cells. *Cancer Res.* **74**, 5782–94 (2014).
- 222 16. Tsai, S., Wear, D. J., Shih, J. W. & Lo, S. C. Mycoplasmas and oncogenesis: persistent  
223 infection and multistage malignant transformation. *Proc. Natl. Acad. Sci. U. S. A.* **92**,  
224 10197–201 (1995).
- 225 17. Rogers, M. B. Mycoplasma and cancer: in search of the link. *Oncotarget* **2**, 271–3 (2011).
- 226 18. Geller, L. T. *et al.* Potential role of intratumor bacteria in mediating tumor resistance to  
227 the chemotherapeutic drug gemcitabine. *Science (80-. ).* **357**, 1156–1160 (2017).
- 228 19. Gazzaniga, F., Stebbins, R., Chang, S. Z., McPeck, M. A. & Brenner, C. Microbial NAD  
229 Metabolism: Lessons from Comparative Genomics. *Microbiol. Mol. Biol. Rev.* **73**, 529–  
230 541 (2009).
- 231 20. Liu, L. *et al.* Quantitative Analysis of NAD Synthesis-Breakdown Fluxes. *Cell Metab.* **27**,

- 232 1067–1080.e5 (2018).
- 233 21. Harasawa, R. *et al.* Rapid detection and differentiation of the major mycoplasma  
234 contaminants in cell cultures using real-time PCR with SYBR Green I and melting curve  
235 analysis. *Microbiol. Immunol.* **49**, 859–63 (2005).
- 236 22. Matheny, C. J. *et al.* Next-Generation NAMPT Inhibitors Identified by Sequential High-  
237 Throughput Phenotypic Chemical and Functional Genomic Screens. *Chem. Biol.* **20**,  
238 1352–1363 (2013).
- 239 23. He, Z. *et al.* A high capacity polymeric micelle of paclitaxel: Implication of high dose  
240 drug therapy to safety and in vivo anti-cancer activity. *Biomaterials* **101**, 296–309 (2016).
- 241 24. Lorson, T. *et al.* Poly(2-oxazoline)s based biomaterials: A comprehensive and critical  
242 update. *Biomaterials* **178**, 204–280 (2018).
- 243 25. Liu, X., Ser, Z. & Locasale, J. W. Development and Quantitative Evaluation of a High-  
244 Resolution Metabolomics Technology. *Anal. Chem.* **86**, 2175–2184 (2014).
- 245 26. Chong, J. *et al.* MetaboAnalyst 4.0: towards more transparent and integrative  
246 metabolomics analysis. *Nucleic Acids Res.* **46**, W486–W494 (2018).
- 247 27. Yaku, K., Okabe, K. & Nakagawa, T. Simultaneous measurement of NAD metabolome in  
248 aged mice tissue using liquid chromatography tandem-mass spectrometry. *Biomed.*  
249 *Chromatogr.* **32**, e4205 (2018).
- 250 28. Frezza, C., Cipolat, S. & Scorrano, L. Organelle isolation: functional mitochondria from  
251 mouse liver, muscle and cultured fibroblasts. *Nat. Protoc.* **2**, 287–295 (2007).

252

253

254 **Acknowledgments**

255 We thank Drs. Traci Hall, Michael Fessler, and Paul Wade, and members of the Li laboratory for  
256 critical reading of the manuscript; We also thank Dr. So Young Kim from Duke University  
257 Genetic and Chemical Screening Services for construction of E2F1 targeting CRISPR construct  
258 and help with the drug screen, and Mr. Michael Johnston, Dr. David Kurtz and the Quality  
259 Assurance Laboratory of National Institute of Environmental Health Sciences for detecting  
260 mycoplasma contamination in our cultured cells.

261

262 **Funding**

263 This research was supported by the Intramural Research Program of National Institute of  
264 Environmental Health Sciences of the NIH to XL (Z01 ES102205).

265

266 **Authors contributions**

267 IS and XL designed the study, analyzed the results and wrote the manuscript. IS performed all  
268 biological experiments with help from EL and WF. JL and JWL performed metabolomic  
269 analysis. JGW and LJD performed targeted analysis of NAD pathway metabolites. CL, MS, and  
270 AVK developed the formulation of STF1188804 for the *in vivo* studies. All authors critically  
271 reviewed the manuscript.

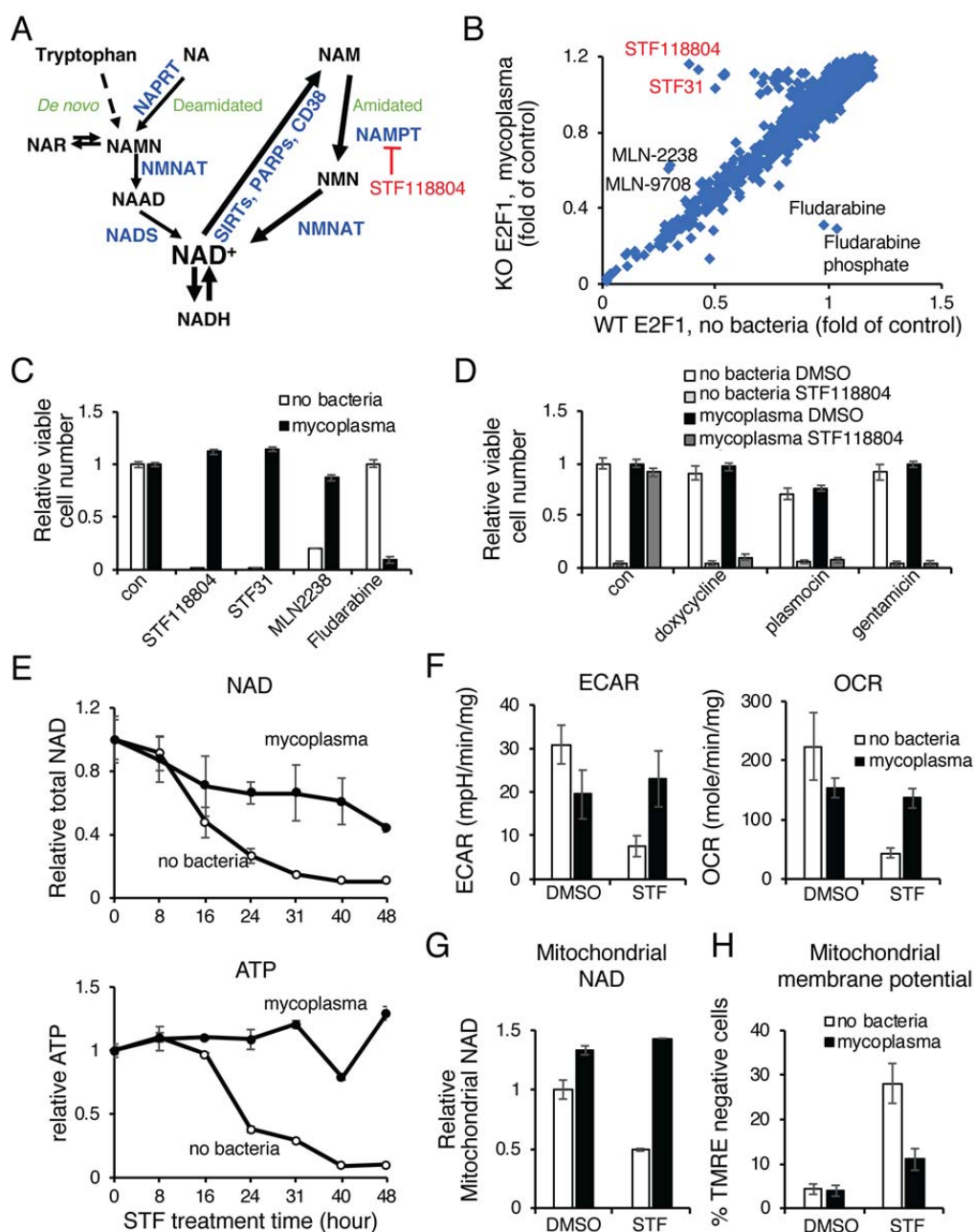
272

273 **Competing interests**

274 Authors declare no competing interests.

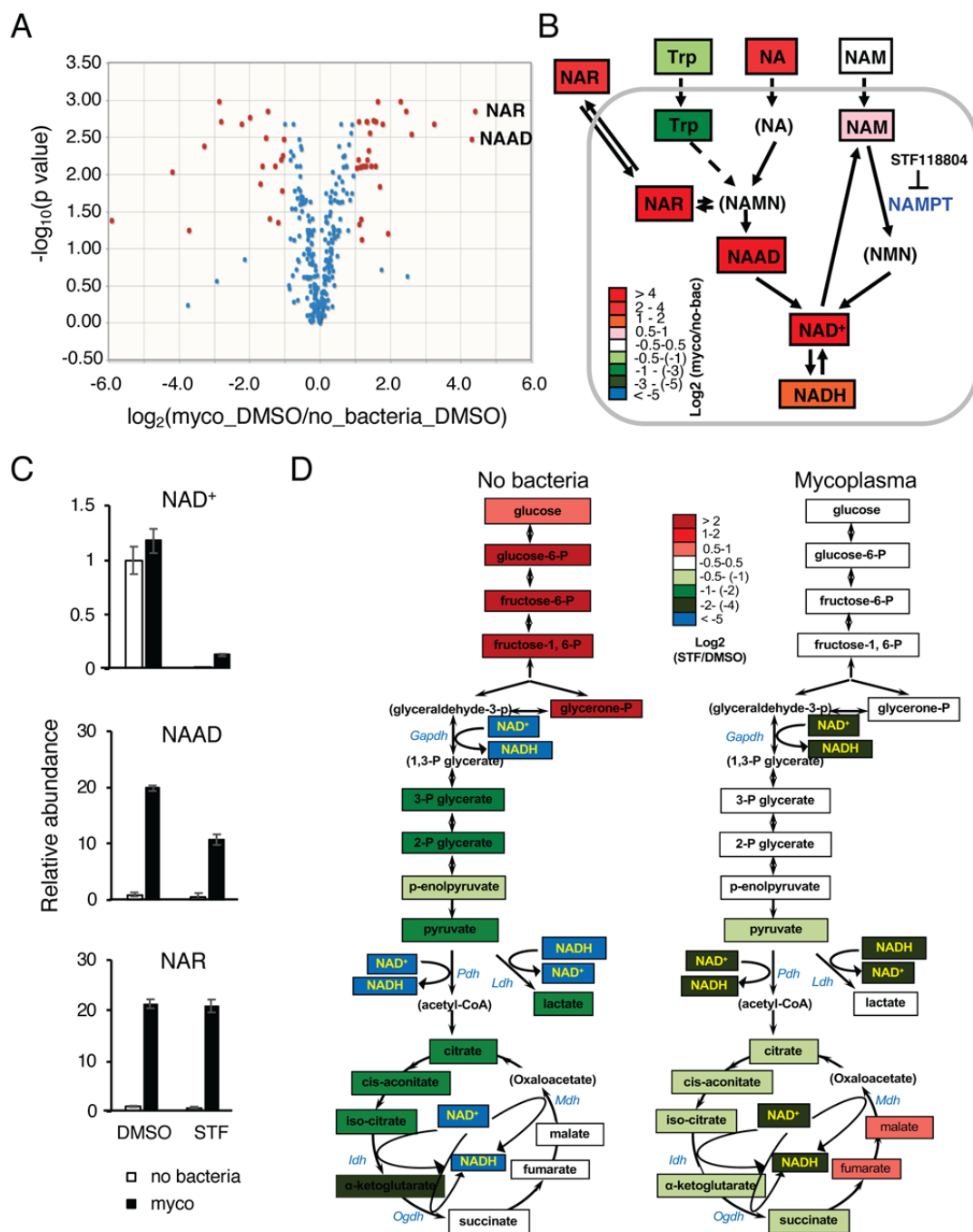
275

276



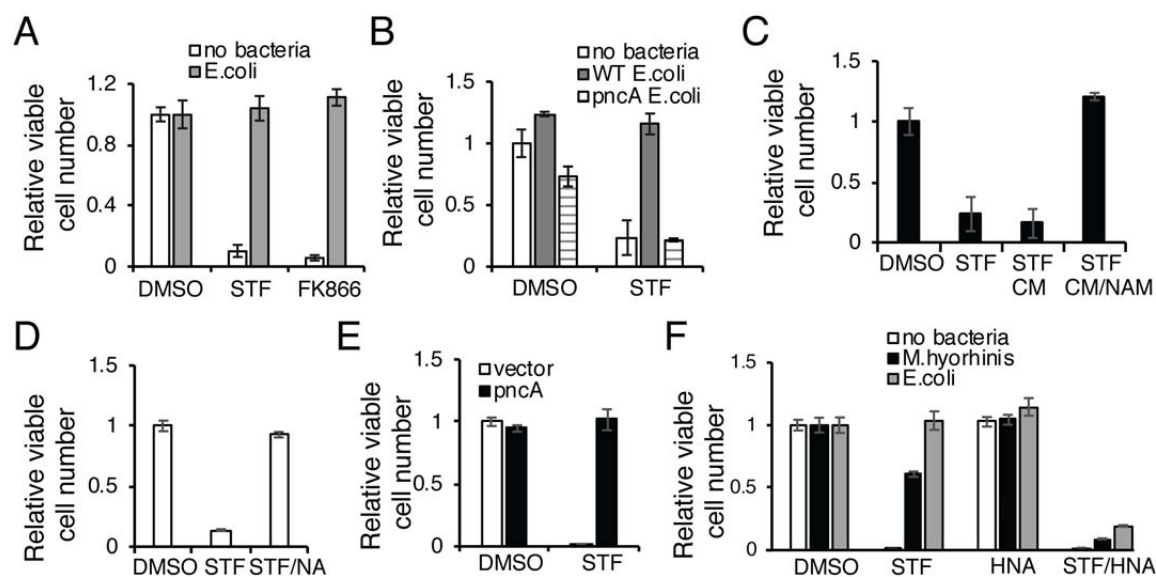
277 **Figure 1. Mycoplasma infection confers host cells with resistance to NAMPT inhibitors by preventing NAD and energy depletion**  
 278 (A) NAD biosynthesis pathway. NAR: nicotinic acid riboside; NAMN: nicotinic acid mononucleotide; NAAD: nicotinic acid adenine dinucleotide; NADS:  
 279 NAD Synthetase; NMNAT: Nicotinamide Nucleotide Adenylyltransferase. (B) Drug screen in H1299. WT and E2F1 KO H1299 cells were treated with 1  $\mu$ M  
 280 compounds from the bioactive compound library and viability was measured 48 hours later by CellTiter-Glo (CTG) assay. E2F1 KO cells were subsequently  
 281 found to be infected with mycoplasma. (C) Mycoplasma infection confers resistance to NAMPT and proteasome inhibitors but sensitizes to fludarabine. CRC119  
 282 cells incubated with a supernatant from a mycoplasma-infected culture or a control medium, and treated with 100 nM STF118804, 1  $\mu$ M STF31, 50 nM  
 283 MLN2238 or 1  $\mu$ M fludarabine or control for 68 hours. (D) Elimination of mycoplasma sensitizes cells to NAMPTi-induced toxicity. Clean and mycoplasma-  
 284 infected CRC119 cells were treated with 1  $\mu$ g/ml doxycycline, 25  $\mu$ g/ml plasmocin, or 400  $\mu$ g/ml gentamicin for 24 hours, then co-treated with antibiotics and  
 285 100 nM STF118804 for an additional 48 hours. (E) Mycoplasma prevent NAMPTi-induced NAD and ATP depletion. Total cellular NAD (NADH + NAD<sup>+</sup>) and  
 286 ATP levels were measured in uninfected (no bacteria) or mycoplasma-infected CRC119 cells treated with 100 nM STF118804 (STF). (F) Mycoplasma prevent  
 287 NAMPTi-induced inhibition of glycolysis (ECAR) and oxidative phosphorylation (OCR). Uninfected clean or mycoplasma-infected CRC119 cells were treated  
 288 with 100 nM STF118804 (STF) for 48 hours. The basal extracellular acidification rate (ECAR) and oxygen consumption rate (OCR) were measured using  
 289 Seahorse instrument. (G) Mycoplasma prevent NAMPTi-induced mitochondrial NAD depletion. Relative levels of mitochondrial total NAD were measured after  
 290 24 hours treatment with 100 nM STF118804 (STF) or DMSO control. (H) Mycoplasma prevent NAMPTi-induced loss of mitochondrial membrane potential.  
 291 Mitochondrial membrane potential loss (% TMRE-negative cells) was measured by flow cytometry after 24 hours treatment with 100 nM STF118804 (STF) or  
 292 DMSO control. All data are means and SD of biological triplicates from representative experiments. Each experiment was repeated at least twice.

293  
294



295 **Figure 2. Mycoplasma induce deamidated NAD precursors and prevent NAMPTi-induced NAD and energy depletion**  
 296 (A) Mycoplasma dramatically increases cellular levels of deamidated NAD precursors. Clean (no bacteria) or M.hyorhinis-infected (myco) CRC119 cells  
 297 were treated with either 100 nM STF118804 or with DMSO control for 24 hours and relative levels of 330 metabolites were determined by LC-MS.  
 298 Volcano plot of metabolites from mycoplasma-infected cells (Myco\_DMSO) vs. uninfected cells (no bacteria\_DMSO). (B) Mycoplasma dramatically  
 299 increase deamidated NAD precursors inside the cells and in the medium upon STF118804 treatment. The log ratios of the relative abundance of  
 300 metabolites in clean and infected cells are represented by color scale. Metabolites in parenthesis were not detected in our LC-MS analysis. (C) Relative  
 301 levels of NAD<sup>+</sup> and the top differential metabolites (NAAD and NAR). (D) Mycoplasma prevent NAMPTi-induced impairment of energy metabolism.  
 302 Relative changes in the levels of glycolysis and TCA cycle metabolites following STF118804 treatment are shown for uninfected (left panel) and  
 303 mycoplasma-infected cells (right panel). The log ratios of the relative abundance of metabolites in indicated pathways in clean and infected cells  
 304 are represented by color scale. Metabolites in parenthesis were not detected in our LC-MS analysis. See also Table S2 for the complete metabolomics data. All  
 305 data are means and SD of biological triplicates from a single experiment.  
 306

307  
308  
309  
310  
311  
312  
313  
314  
315  
316  
317  
318  
319  
320



321 **Figure 3. Bacteria rescue NAMPTi-induced toxicity through nicotinamidase PncA**  
 322 (A) *E. coli* protect cells from NAMPTi-induced toxicity. CRC119 cells were cultured with or without *E. coli* in the presence of 1  $\mu$ g/ml  
 323 gentamycin to prevent bacterial overgrowth. Cells were treated with 100 nM STF118804, 50 nM FK866, or with DMSO control for 42 hours. (B)  
 324 *E. coli* protect cells from NAMPTi-induced toxicity through PncA. CRC119 cells were treated with 100 nM STF118804 or DMSO control for 48  
 325 hours, then treated with control medium, live WT *E. coli*, or *pncA* KO *E. coli* for additional 24 hours. (C) *E. coli*-provided protection from  
 326 NAMPTi require NAM. *E. coli* were incubated in EBSS medium with or without nicotinamide (NAM) for 3 hours, then removed by filtering  
 327 through 0.2  $\mu$ m filter. The conditioned media (CM) were added for an additional 24 hours to CRC119 cells that were pre-treated for 24 hours  
 328 with 100 nM STF118804. (D) NA protects cells from NAMPTi-induced toxicity. CRC119 cells were treated with 100 nM STF118804 with or  
 329 without 100  $\mu$ M nicotinic acid (NA) for 48 hours. (E) Overexpression of PncA protects cells from NAMPTi-induced toxicity. CRC119  
 330 transfected with a control vector or a construct expressing *E. coli pncA* were treated with 100 nM STF118804 (STF) or DMSO control for 72  
 331 hours. (F) Blocking the deamidated NAD biosynthesis by HNA abolishes bacteria-provided protection from NAMPTi. CRC119 cells cultured  
 332 with clean medium, or medium containing *E. coli*, or *Mycoplasma hyorhinitis* were treated with 100 nM STF118804, 1 mM of HNA or their  
 333 combination for 66 hours. Cell viability in (A-F) was measured by CTG assay. All data are means and SD of biological triplicates from  
 334 representative experiments. Each experiment was repeated at least twice.  
 335  
 336



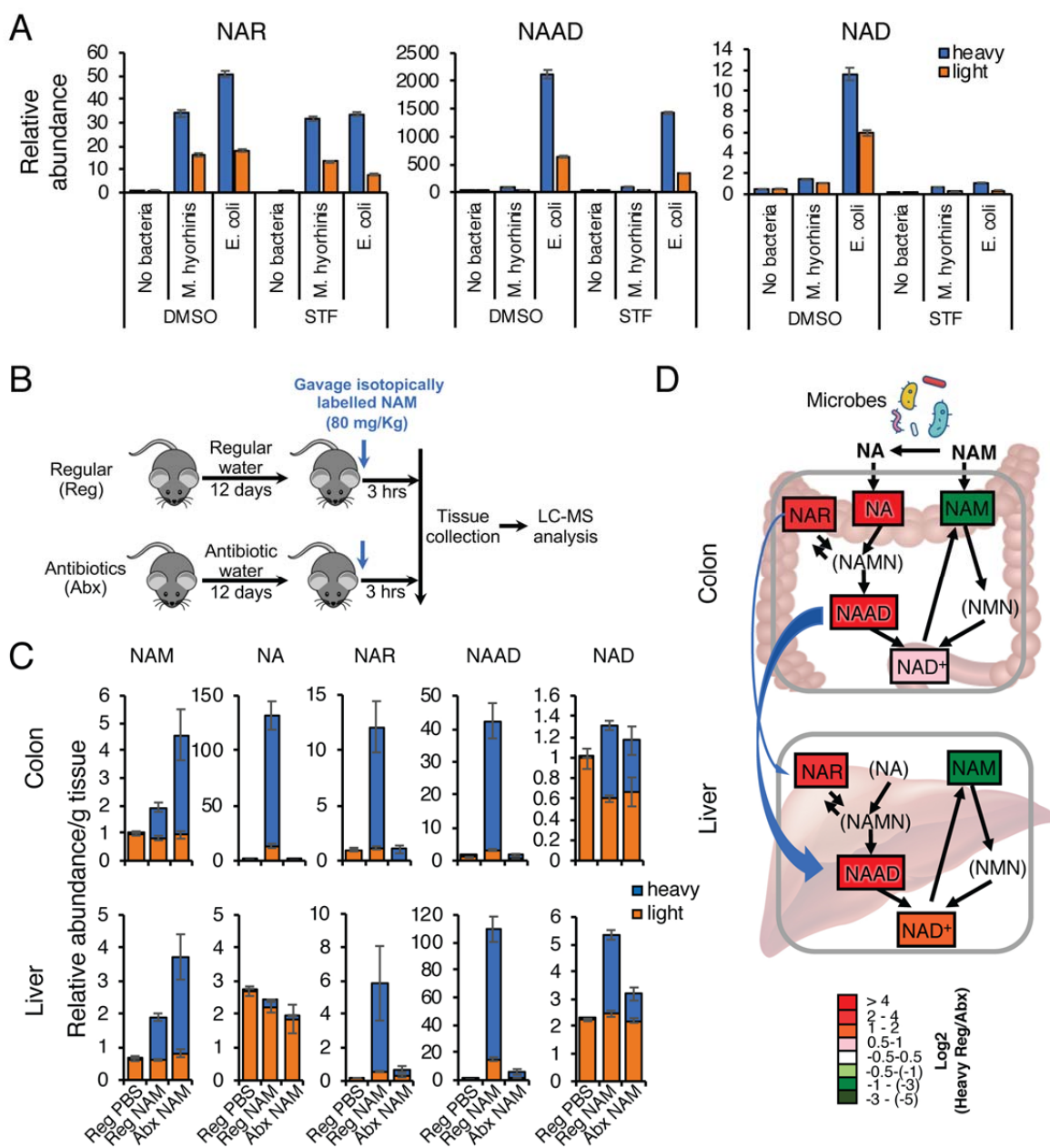


**Figure 4. Bacteria boost incorporation of NAM into metabolites in the deamidated NAD salvage pathway and NAD *in vitro* and *in vivo*.**

(A) Bacteria augment incorporation of NAM into metabolites in the deamidated NAD salvage pathway and NAD. CRC119 cells were infected with the indicated bacteria and treated with 200 nM STF118804 or DMSO control for 24 hours in the presence of 5 mg/l NAM labeled with four deuterium atoms on the pyridine ring. The relative abundance of the indicated unlabeled (light) and labeled (heavy) metabolites was measured by LC-MS. (B-D) Gut microbiota are critical to incorporate dietary NAM into metabolites in the deamidated NAD salvage pathway and NAD *in vivo*. (B) Schematic of the experiment. C57BL/6J mice were treated with either regular water (Reg) or antibiotics-containing water (Abx) for 12 days to deplete gut microbiota. They were then gavaged with 80 mg/kg of isotopically labeled NAM or with PBS control, and dissected three hours later. (C) Relative abundance of unlabeled (light) and labeled (heavy) NAD pathway metabolites in colons and livers were measured by LC-MS (n=5-6 mice/group). (D) Gut microbiota systemically boost the flux of dietary NAM into NAD through the deamidated salvage pathway *in vivo*. The relative abundance of isotopically labeled specific metabolite in colons and livers of regular (Reg) and antibiotics-treated (Abx) mice is normalized to the total level of this metabolite in colons of regular mice. The log ratios of the relative abundance are represented by color scale. Metabolites in parenthesis were not detected in the LC-MS analysis. Data are means and SD from a single in-vivo experiment with 5-6 mice/group.

337  
338  
339  
340  
341  
342  
343  
344  
345  
346  
347  
348  
349  
350  
351  
352  
353

354

## 355 **Methods**

### 356 Cell culture, infections and chemicals

357 H1299 and 293T cells were obtained from Duke University cell culture facility. HCT116 cells  
358 were from ATCC. CRC119 and CRC240 cells were a gift from Dr. David Hsu (Duke  
359 University). All cells were grown in RPMI medium with 10% fetal bovine serum supplemented  
360 with penicillin and streptomycin. For chronic mycoplasma infection, cells were infected once  
361 with *Mycoplasma Hyorhina* (ATCC® 17981™) and then passaged as usual. For *E.coli*  
362 experiments, penicillin and streptomycin in growth medium were substituted by 1 µg/ml  
363 gentamycin as we found this concentration to be bacteriostatic. Cells were infected with 1:1000  
364 dilution of overnight stationary phase K12 *E.coli* culture (*E. coli* Keio Knockout Parent Strain  
365 BW25113, #OEC5042 or *pncA* KO #OEC4987-200827138, Dharmacon). Separate tissue  
366 culture reagents bottles and incubator shelves (in addition to secondary containment in larger  
367 dishes) were used for the infected cultures. Following the initial discovery of mycoplasma in  
368 H1299 E2F1 KO cells, mycoplasma contamination status of all cultures was monitored by real-  
369 time PCR monthly<sup>21</sup>.

370 STF118804, STF31, FK866, MLN2238, and fludarabine were purchased from Selleckchem. For  
371 the *in-vivo* study, STF118804 was purchased from Medchemexpress.

372 Plasmocin was purchased from Invivogen. All other chemicals were purchased from Sigma.

373

374

### 375 Drug Screen

376 Drug screen was performed at Duke University Genetic and Chemical Screening Services.

377 Wildtype or E2F1 knockout H1299 cells were plated using a Matrix WellMate onto 384-well  
378 plates that had been stamped using a Labcyte Echo Acoustic Dispenser with the  
379 Bioactive compound library (Selleckchem), for a final concentration of 1.25  $\mu$ M in duplicate  
380 plates. Cells were incubated for 48 hours and assayed for cell viability with Cell Titer-Glo  
381 (Promega). All well values were normalized to the average of DMSO control wells found on  
382 each plate. Figure 1A shows average normalized values of duplicate plates. Full screen results  
383 can be found in Table S1.

384

### 385 Animal experiments

386 All animal work was approved by the Institutional Animal Care and Use Committee of the  
387 National Institute of Environmental Health Sciences.

388 For xenograft experiment,  $2 \times 10^6$  *M. hyorhinis*-positive or negative HCT116 human colon  
389 carcinoma cells were subcutaneously injected into each flank of 6 week old female Nu/J mice  
390 (#002019, Jackson labs). We had eight mice per treatment group and all mice developed at least  
391 one tumor. Tumor length and width were measured by caliper and tumor volume was calculated  
392 using the formula  $V = \text{length} \times \text{width}^2 / 2$ . Treatment with 15 mg/kg twice daily subcutaneous  
393 injections of STF118804 or vehicle control was initiated when the largest tumor reached 200  
394  $\text{mm}^3$ .

395 Due to solubility problem of the published STF118804 formulation<sup>22</sup> we developed a new  
396 formulation using block co-polymer micelles. The amphiphilic triblock copolymer [P(MeOx<sub>35</sub>-*b*-  
397 BuOx<sub>20</sub>-*b*-MeOx<sub>34</sub>), Mn=8.4 kg/mole, PDI =1.18] was synthesized by living cationic ring-  
398 opening polymerization<sup>23,24</sup>. Briefly, pre-determined amounts of polymer and STF118804 were  
399 dissolved in acetone and mixed well at 1:10 drug:polymer ratio, followed by complete

400 evaporation of acetone to form a thin film. The formed thin film was rehydrated with appropriate  
401 amount of distilled water and sonicated for 10 min. To remove residual solid STF118804 (if  
402 any), the samples were centrifuged at 10,000 g for 3 min and the supernatant was obtained and  
403 lyophilized. The lyophilized samples were rehydrated with normal saline immediately before  
404 use. The concentration of STF118804 in polymeric micelles was determined by reverse-phase  
405 high-performance liquid chromatography using an Agilent Technologies 1200 series HPLC  
406 system equipped with UV detector and a Nucleosil C18 5  $\mu\text{m}$  column (250 mm  $\times$  4.6 mm).  
407 STF118804 was eluted with ACN/water; 70/30 as mobile phase, at a flow rate of 1mL/min and  
408 detected at 310nm. The concentration of STF118804 was calculated using a linear calibration  
409 curve against standard STF118804 solution.

410 Mice were sacrificed after two weeks of treatment or earlier when tumors reached 1000 mm<sup>3</sup> as  
411 required by the animal protocol.

412 For isotopic tracing experiment, eight weeks old C57BL/6 male mice were either given regular  
413 water or autoclaved water containing antibiotic cocktail (1 g/l ampicillin, 1 g/l neomycin, 1 g/l  
414 metronidazole, 500 mg/l vancomycin) for twelve days. Fecal DNA was isolated using QIAamp  
415 DNA Stool Mini Kit (Qiagen) and microbiota depletion was verified by qPCR using 16S V3  
416 sequencing primers (5'-tcgtcggcagcgtcagatgtgtataagagacagccagactcctacgggagggcag-3';

417 5'-gtctcgtgggctcggagatgtgtataagagacagcgtattaccgggctgctg-3').

418 Control and microbiota-depleted mice were treated with oral gavage of 80 mg/kg nicotinamide  
419 labeled with 4 deuterium atoms on the pyridine ring (D4-NAM). Additional control group of  
420 mice also received a PBS gavage. Gavages were staggered and were given alternating between  
421 control and microbiota-depleted mice to avoid any experimental bias. Mice were sacrificed three

422 hours after gavage. Colons were flushed and flash frozen in liquid nitrogen along with livers.  
423 Samples were stored at -80 degrees before processing. Each treatment group had 5-6 mice.

424

#### 425 Plasmids

426 For CRISPR-Cas9-mediated E2F1 knockout, gRNA sequence 5'-ggagatgatgacgatctgcg-3'  
427 targeting exon 1 of E2F1 was cloned into LentiCRISPR v.2 (Addgene, #52961).

428 For inducible knockdown of E2F1, shRNAmir insert from E2F1-targeting pGIPZ (Dharmacon,  
429 #V3LHS\_393591) was cloned into pTRIPZ vector (Dharmacon) with MluI and XhoI to produce  
430 pTRIPZ-shE2F1.

431 For overexpression of HA-PncA, *pncA* gene was amplified from *E.coli* genomic DNA using  
432 caccctcgaggccccctcgcgccctgttactg and caccgeggccgcttaccctgtgtctcttcccag primers and cloned  
433 into pcDNA3-HA plasmid using XhoI and NotI sites. The cloned *pncA* sequence was verified by  
434 Sanger sequencing.

435

#### 436 E2F1 knockdown and PncA overexpression

437 For E2F1 knockdown, lentiviral particles were produced using 293T cells co-transfected with  
438 pMD2.G (Addgene #12259), and psPAX2 (Addgene #12260) and LentiCRISPR v.2 targeting  
439 construct for E2F1 knockout or pTRIPZ-shE2F1 for inducible E2F1 knockdown using Mirus  
440 TransIT-LT1 Transfection Reagent. Target cells were infected with lentivirus-containing  
441 supernatant and selected with 2.5 µg/ml puromycin. Expression of the inducible shRNA from  
442 pTRIPZ-shE2F1 was induced by addition of 1 µg/ml doxycycline.

443

444 For PncA overexpression, CRC119 cells were transiently transfected with pcDNA-HA-pncA  
445 using GenJet Ver.II transfection reagent (Signagen).

446

#### 447 Western blot

448 Cell pellets were lysed with RIPA buffer containing Complete Mini protease inhibitor cocktail  
449 (Roche Diagnostics). Proteins were resolved on 4–20% gradient SDS-PAGE, transferred to  
450 PVDF membranes and probed with antibodies for E2F1 (Santa Cruz Biotechnologies, sc-251),  
451 GAPDH (Cell Signaling Technology, 2118S), alpha-tubulin (Abcam, Ab7291), HA (Santa Cruz  
452 Biotechnologies, sc-7392).

453

#### 454 NAD, ATP and viability enzymatic assays

455 For all assays, cells were plated at 10,000 cells per well in clear bottom white plates (Corning,  
456 #3610). For enzymatic measurement of total NAD, NAD/NADH-Glo™ kit (Promega) were  
457 used. CellTiter-Glo® (Promega), which measures cellular ATP, was used for ATP kinetics (Fig.  
458 2A) and as a proxy for cell number (viability).

459

#### 460 Metabolomics analysis using LC-MS

461 Cells were grown in 6-well plates in triplicates and treated with 100 nM STF118804 or DMSO  
462 control for 24 hours. After collection of medium samples, cells were briefly washed with saline  
463 and metabolites were extracted by scraping cells on dry ice into cold 80% methanol/20% water.  
464 Plates were incubated at -80 degree for 15 minutes and extracts transferred into microcentrifuge  
465 tubes. Following centrifugation at 14000 rpm for 10 minutes, supernatants were transferred to  
466 new tubes and dried in a vacuum concentrator at room temperature. The dry pellets were

467 reconstituted into 30  $\mu$ l (per 3 mg tissue) sample solvent (water:methanol:acetonitrile, 2:1:1, v/v)  
468 and 3  $\mu$ l was further analyzed by liquid chromatography-mass spectrometry (LC-MS).

469 For tissue analysis, frozen tissues were pulverized in a mortar in liquid nitrogen and stored on  
470 dry ice. 20-30 mg of tissue powder was weighed, extracted in cold 80% methanol/20% water  
471 and processed as described for cells.

472  
473 LC-MS method for metabolomics- Ultimate 3000 UHPLC (Dionex) is coupled to Q Exactive  
474 Plus-Mass spectrometer (QE-MS, Thermo Scientific) for metabolite profiling. A hydrophilic  
475 interaction chromatography method (HILIC) employing an Xbridge amide column (100 x 2.1 mm  
476 i.d., 3.5  $\mu$ m; Waters) is used for polar metabolite separation. Detailed LC method was described  
477 previously<sup>25</sup> except that mobile phase A was replaced with water containing 5 mM ammonium  
478 acetate (pH 6.8). The QE-MS is equipped with a HESI probe with related parameters set as  
479 below: heater temperature, 120 °C; sheath gas, 30; auxiliary gas, 10; sweep gas, 3; spray voltage,  
480 3.0 kV for the positive mode and 2.5 kV for the negative mode; capillary temperature, 320 °C; S-  
481 lens, 55; A scan range (m/z) of 70 to 900 was used in positive mode from 1.31 to 12.5 minutes.  
482 For negative mode, a scan range of 70 to 900 was used from 1.31 to 6.6 minutes and then 100 to  
483 1,000 from 6.61 to 12.5 minutes; resolution: 70000; automated gain control (AGC),  $3 \times 10^6$  ions.  
484 Customized mass calibration was performed before data acquisition. Metabolomics data analysis-  
485 LC-MS peak extraction and integration were performed using Sieve 2.2 (Thermo Scientific). The  
486 peak area was used to represent the relative abundance of each metabolite in different samples.  
487 Missing values were handled as described in <sup>25</sup>. MetaboAnalyst package was used for the PCA  
488 analysis, the differential metabolite presentation by volcano plot and for metabolic pathways  
489 enrichment analysis <sup>26</sup>.

490  
491 For targeted analyses of compounds from the NAD pathway, a method based upon the report  
492 from Yaku, et al. was developed <sup>27</sup>. Data were acquired on a Q Exactive Plus mass spectrometer  
493 (QE-MS, Thermo Scientific) interfaced with a Vanquish (Thermo Fisher) UHPLC system.  
494 Reverse-phase chromatography was performed using a CORTECS C18 column (100 x 2.1 mm  
495 i.d., 1.6  $\mu$ m; Waters) with solvent A being 5 mM ammonium formate in water (pH 6.5) and  
496 solvent B being methanol and a flow rate of 150  $\mu$ L/minute. The LC gradient included a ramp  
497 from 0% to 42% B over the first 6 minutes followed by a ramp to 95% over the next minute. A 3  
498 minute hold at 95% was followed by a return to 0% B over the next 0.5 minutes. The run was  
499 completed with a 9.5 minute recondition at 0% B. For the mass spectrometry, a PRM method  
500 was employed with a segmented include list for the masses of the metabolites of interest and their  
501 optimized normalized collision energies. The QE-MS was equipped with a HESI source used in  
502 the positive ion mode with the following instrument parameters: sheath gas, 40; auxiliary gas, 10;  
503 sweep gas, 1; spray voltage, 3.5 kV; capillary temperature, 325  $^{\circ}$ C; S-lens, 50; scan range (m/z) of  
504 70 to 1000; 2 m/z isolation window; resolution: 17,500; automated gain control (AGC),  $2 \times 10^5$   
505 ions; and a maximum IT of 200 ms. Mass calibration was performed before data acquisition using  
506 the LTQ Velos Positive Ion Calibration mixture (Pierce). PRM data were processed using either  
507 the Qual Browser application or the Xcalibur processing feature in the Xcalibur software suite  
508 (Thermo Scientific). Extracted ion chromatograms for fragment ions were drawn for each of the  
509 NAD metabolites in their respective channels at their appropriate elution times and areas under the  
510 peak calculated and used to represent the relative abundance of each metabolite in the samples.  
511 Peak areas were normalized to tissue weight.

512



### 513 RNA isolation and RT-PCR

514 Xenograft tumors were frozen and powdered in liquid nitrogen using mortar and pestle. Total  
515 RNA was isolated using RNeasy Kit (Qiagen) and reverse-transcribed using High-Capacity  
516 cDNA Reverse Transcription Kit (ThermoFisher Scientific). Real-time PCR was performed on  
517 CFX96 real time PCR instrument (Bio-Rad) using iQ SYBR Green SuperMix (Bio-Rad) with  
518 the following primers: E2F1 (cggcgcatctatgacatcac, gtcaaccctcaagccgctc),  
519 CCNA2 ( cctgcgttcaccattcatgt, caggcatcttcacgctctat), GAPDH (accactcctccaccttga,  
520 ctggtgctgtagccaaattcgt).

521

### 522 Mitochondrial membrane potential loss

523 Cells were trypsinized, stained with 100 nM tetramethylrhodamine ethyl ester (TMRE) and  
524 analyzed by flow cytometry on LCR II instrument (BD Biosciences).

525

### 526 NAD measurement in isolated cytosolic and mitochondrial fractions

527 Mitochondrial and cytosolic fraction were isolated according to<sup>28</sup> and relative NAD/NADH  
528 content was determined with NAD/NADH Quantitation Kit (Sigma, MAK037). NAD values  
529 were normalized to protein content determined by BCA kit (ThermoFisher Scientific).

530

### 531 Bioenergetic profiling

532 Extracellular acidification rate (ECAR) and oxygen consumption rate (OCR) were analyzed on  
533 Seahorse XFe96 Analyzer (Agilent) using Seahorse XF Cell Mito Stress Test Kit and Glycolysis  
534 Stress Test Kit (Agilent). Following completion of the analysis, protein content in each well was

535 determined by BCA kit (ThermoFisher Scientific) and used for normalization of the raw ECAR

536 and OCR values.

537

538